Prediction of Warner-Bratzler shear force, intramuscular fat, drip-loss and cook-loss in beef via Raman spectroscopy and chemometrics

Raquel Cama-Moncunill[a], Jamie Cafferky[a,b], Caroline Augier[a], Torres Sweeney[b], Paul Allen[a], Alessandro Ferragina[a], Carl Sullivan[c], Andrew Cromie[d], Ruth M. Hamill[a,*]

[a] Department of Food Quality and Sensory Science, Teagasc Food Research Centre, Ashtown, Dublin 15, Ireland
[b] School of Veterinary Medicine, University College Dublin, Belfield, Dublin 4, Ireland
[c] School of Food Science and Environmental Health, TU Dublin - City Campus, Cathal Brugha Street, Dublin 1, Ireland
[d] Irish Cattle Breeders Federation, Highfield House, Bandon, Co. Cork, Ireland

ABSTRACT

Rapid prediction of beef quality remains a challenge for meat processors. This study evaluated the potential of Raman spectroscopy followed by chemometrics for prediction of Warner-Bratzler shear force (WBSF), intramuscular fat (IMF), ultimate pH, drip-loss and cook-loss. PLS regression models were developed based on spectra recorded on frozen-thawed day 2 *longissimus thoracis et lumborum* muscle and validated using test sets randomly selected 3 times. With the exception of ultimate pH, models presented notable performance in calibration (R^2 ranging from 0.5 to 0.9; low RMSEC) and, despite variability in the results, promising predictive ability: WBSF (RMSEP ranging from 4.6 to 9 N), IMF (RMSEP ranging from 0.9 to 1.1%), drip-loss (RMSEP ranging from 1 to 1.3%) and cook-loss (RMSEP ranging from 1.5 to 2.9%). Furthermore, the loading values indicated that the physicochemical variation of the meat influenced the models. Overall, results indicated that Raman spectroscopy is a promising technique for routine quality assessments of IMF and drip-loss, which, with further development and improvement of its accuracy could become a reliable tool for the beef industry.

1. Introduction

Besides safety and nutritional content, beef consumers expect a satisfying eating experience. This means that beef and especially premium beef cuts must embrace a series of characteristics in flavour, texture, tenderness, juiciness and appearance in order to meet consumer expectations (Hocquette et al., 2014; Troy & Kerry, 2010). These characteristics, which together determine the overall eating quality of beef, are affected by several factors, typically classified as: intrinsic (e.g. breed, sex and age) and extrinsic (e.g. season, feeding, slaughtering and post-slaughter management) (Gagaoua, Picard, Soulat, & Monteils, 2018). Thus, variations in these factors may cause unpredictable eating experiences that can lead to consumer disappointment, and even dissatisfaction (McCarthy, Henchion, White, Brandon, & Allen, 2017).

Several objective indicators have been developed to provide instrumental information on the eating quality of beef. Texture, especially first bite tenderness is one of the most important factors determining consumer acceptability in beef steak and can be instrumentally estimated through shear-force measurements such as Warner-Bratzler shear force (WBSF) (AMSA, 2015). The amount of intramuscular fat

(IMF) is also considered an indicator of beef eating quality as high levels of IMF have been associated with improved tenderness, juiciness and flavour (Corbin et al., 2015; Hocquette et al., 2014; Webb & O'Neill, 2008). The ability to retain water—referred to as water holding capacity (WHC)—is also a key aspect as it affects the visual acceptability, juiciness and tenderness of beef (Barbera, 2019; Modzelewska-Kapituła, Kwiatkowska, Jankowska, & Dąbrowska, 2015). Furthermore, water-holding capacity has an additional value to processors in terms of its relationship with carcass yield (Di Luca, Mullen, Elia, Davey, & Hamill, 2011; Reardon, Mullen, Sweeney, & Hamill, 2010). Ultimate pH is an important indicator as it has a relationship to water-holding capacity and tenderness (Honikel, 2014a). However, classic measurements of WBSF, IMF and WHC are not amenable to routine analyses of beef quality in each carcass as these methods are destructive, time intensive and require complex sample preparation. Consequently, current challenges for the meat sector include the development and implementation of non-invasive tools capable of providing timely and reliable information on beef quality on an individual basis. Furthermore, this information could be used to inform consumers about the quality of the product, as well as in breeding programmes for the improvement of

beef eating quality (Cecchinato, De Marchi, Penasa, Albera, & Bittante, 2011).

Raman spectroscopy is a vibrational technique which offers speed, non-invasive measurement and minimal sample preparation requirements as advantages (Ana M. Herrero, 2008; Gremlich and Yan, 2000). Raman spectroscopy is based on the inelastic scattering of light resulting from the interaction between a laser light and the molecules of a sample (Li-Chan, Griffiths, & Chalmers, 2010). Light inelastically scattered, which refers to photons that have been scattered from the sample with a different energy level/frequency than the incident light (laser), contains information about fundamental molecular vibrations (Berhe, Engelsen, Hviid, & Lametsch, 2014; Vankeirsbilck et al., 2002). Thus, Raman spectroscopy registers the vibrational signal of the scattering species of a sample proving information about its molecular composition and structure (Schmidt, Scheier, & Hopkins, 2013).

During the last decade, Raman spectroscopy has received increasing interest for many food applications. In the field of meat quality, few studies have been conducted to examine the potential of the technique, but those that have been done suggest the technology has merit for this field. For example, Raman spectroscopy was used to predict various meat-quality indicators such as pH, colour and IMF of pork (Andersen, Wold, Gjerlaug-Enger, & Veiseth-Kent, 2018; Nache, Hinrichs, Scheier, Schmidt, & Hitzmann, 2016; Scheier, Bauer, & Schmidt, 2014), beef (Fowler, Schmidt, van de Ven, & Hopkins, 2018; Nian et al., 2017) and lamb (Fowler, Schmidt, van de Ven, Wynn, & Hopkins, 2015). Best results were obtained for the prediction of pH_u (R^2cv = 0.65) (Scheier et al., 2014) and IMF (R^2cv = 0.73) (Andersen et al., 2018) of pork. The technique was also evaluated for the prediction of instrumental tenderness and sensorial attributes of beef (Bauer, Scheier, Eberle, & Schmidt, 2016; Beattie, Bell, Farmer, Moss, & Patterson, 2004; Zhao et al., 2018) and lamb (Fowler, Schmidt, van de Ven, Wynn, & Hopkins, 2014a; Fowler, Schmidt, Van de Ven, Wynn, & Hopkins, 2014b).

The objective of this study was to assess the potential of Raman spectroscopy combined with chemometric techniques to provide a level of information on the objective meat quality of beef LTL using samples collected at day 2 post-mortem. To this end, prediction models for instrumental tenderness (WBSF), IMF, drip-loss and cook-loss were developed from Raman spectra.

2. Materials and methods

2.1. Samples

Crossbred bull and steer progeny (n = 110, 18 ± 4 months old) from elite Irish beef breed artificial insemination (AI) bulls were obtained and reared under the same feeding and environmental conditions by the Irish Cattle Breeders Federation Tully Progeny Test Centre (Tully, Kildare, ROI). Animals were slaughtered in 8 different batches at a time between February 2014 and May 2017 in a commercial plant by electrical stunning (50 Hz) followed by exsanguination. Between 40 and 60 min post exsanguination, carcasses were split in half and placed in the chill. Four steaks with a thickness of 2.54 cm were removed sequentially from the right-side *longissimus thoracis et lumborum* (LTL) muscle 48 h post-mortem starting at the rump end. Steaks were then vacuum packaged and numbered so that subsequent trait analysis was conducted on a consistent location within LTL muscle. Steaks were frozen at −20 °C after 2 days or 14 days of ageing in a chill at 4 °C depending on the respective trait to be determined.

2.2. Ultimate pH

Ultimate pH (pH_u) was collected from 109 *longissimus* muscles at 48 h post-mortem using a calibrated pH meter (Hanna HI 9125 pH meter, Woonsocket, RI 02895, USA).

2.3. Drip-loss

Drip-loss was analysed on 81 fresh steaks aged for 2 days following the procedure of Honikel & Hamm (1994b). From each steak, a piece of meat (2.5 cm thick, 7.5 cm long and 5 cm wide) was selected avoiding connective tissue and large areas of fat to secure representative samples. Selected pieces of meat were lightly blotted with tissue paper, weighed accurately to two decimal places (initial weight ∼ 100 g ± 2 g) and suspended in an expanded clear plastic bag, ensuring that there was no contact between the sample and the bag. Samples were suspended in a 4 °C chill room for 96 h. Afterwards, samples were lightly blotted with a tissue and re-weighed (final weight). The difference between initial and final weight was determined to two decimal places. Drip-loss was expressed as a percentage of initial weight of the steak.

2.4. Intramuscular fat (IMF)

IMF content was determined on 93 steaks that were aged for 2 days and then frozen at -20C until analysis. Thawing was conducted within the vacuum bag in a circulating water bath at 10 to 15 °C for approximately 45 min. Steaks were then trimmed of external fat, cut into cubes of approximately 2.5 × 2.5 cm and homogenised to a fine consistency using a RobotCoupe R2 blender. Two grams of homogenised meat were selected for analysis. Intramuscular fat was measured using a Smart System-5 microwave moisture drying oven and an NMR Smart-Trac rapid fat analyser (CEM Corporation, USA) following the AOAC Official Methods 985.14 & 985.26, (AOAC International, 1995). Results were expressed as percentage of IMF (% *w/w*).

2.5. Cook-loss

Cook-loss was measured on 110 thawed steaks aged for 14 days. Thawing was performed within unsealed plastic vacuum bags in a circulating water bath at 10 to 15 °C. Steaks were trimmed of external fat, blotted lightly with tissue paper to remove moisture and weighed (initial weight). Steaks were then cooked in a water bath (Grant Instruments Ltd., England) set at 72 °C until reaching an internal core temperature of 70 °C. The internal temperature of the steaks was monitored with a temperature probe (Eirelec Ltd., Ireland). Once cooked, samples were cooled to room temperature, lightly blotted with tissue paper and re-weighed (final weight). The difference between initial and final weight was determined and expressed as a percentage of the initial (raw) weight of the steak.

2.6. Warner-Bratzler Shear Force (WBSF)

Warner-Bratzler Shear Force (WBSF) analysis was carried out on 110 tempered (4 °C, overnight) steaks used for determining the cook-loss (14-day post-mortem) according to AMSA guidelines (AMSA, 2015). Measurements were conducted using an Instron 4464 Universal testing machine (Instron Ltd., Buckinghamshire, UK) set with a load cell of 500 N and a cross head speed of −50 mm/min.

For each steak, seven cores of 1.27 cm were sheared perpendicular to the fibre direction. The maximum peak force recorded during analysis was reported as Newton (N) shear force. Final shear force values were computed excluding the highest and lowest measurements, consisting, therefore, of the average of 5 measurements (5 cores). System control and data analysis was performed using the software provided by the manufacturer: Bluehill®2 (Instron Ltd., Buckinghamshire, UK).

2.7. Raman spectroscopy

Raman spectral data was collected on steaks that were aged for 2 days and then frozen at −20 °C until analysis. Thawing was conducted in bag in a circulating water bath at 10 to 15 °C for

approximately 45 min. Measurements were performed immediately after removing vacuum package, trimming external fat and connective tissue, and carefully blotting the surface of the samples with a tissue.

Spectral acquisition was performed using a DXR SmartRaman spectrometer (ThermoFisher Scientific UK Ltd., Loughborough, UK) equipped with a diode laser operating at 780 nm; a charge coupled device (CCD) detector and a universal platform sampling (UPS) accessory with a slit-aperture of 50 μm. Spectral measurements comprised the recording of Raman intensity, expressed as counts per second (cps), over the 250–3381 cm^{-1} Raman shift range with 2 cm^{-1} interval. The scanning settings employed were: 120 mW laser power, 15 s exposure time and 10 exposures. Each sample was scanned 10 times at random locations of its surface and on both sides (5 scans per side). All samples were scanned in random order at room temperature (~20 °C). The Raman system was controlled with the supplied OMNIC software v9.2.98 (ThermoFisher Scientific UK Ltd., Loughborough, UK). Cosmic spikes were automatically removed by the software.

2.8. Spectral pre-processing and data analysis

Spectral pre-processing and data analysis were performed in R (R Core Team, 2018) with the use of R commands and packages, including; *baseline*, *signal*, *EMSC*, *pls* and *plsVarSel*, as well as other in-house functions.

Various Raman spectra presented spikes at around 1100 cm^{-1} with decreasing intensity over a few consecutive Raman spectra (sample replicates). This phenomenon was identified as blooming effect, which occurs when the amount of generated electrons is larger than the charge packet of the CCD detector (Ryabchykov et al., 2016). Blooming effect was corrected by linear interpolation of the region from 1093.059 to 1104.63 cm^{-1}.

Calculations were based on Raman shift ranges from 3100 to 700 cm^{-1} as low signal-to-noise ratio was observed outside this range. Particularly, two ranges were evaluated: 3100–700 cm^{-1}, and 1800–700 cm^{-1}. Prior to spectral pre-processing and averaging the scans/replicates recorded per sample, the raw data set was investigated for outliers. Spectral outliers were first identified by principal component analysis (PCA) using a 99% confidence ellipse on the score plot of the 3rd and 4th components as the first and second component represent the general structure/information of all spectra (de Groot et al., 2001). 14 spectral points were identified as possible outliers, which were then plotted together with their 9 respective replicates. From these 14 spectra, only those that clearly presented differences in shape or intensity were identified as outliers. A total of 12 replicates (1%) from 11 different samples were discarded. Similarly, reference data points that lied outside 1.5 * IQR (interquartile range) were not included in the models (Wilcox, 2010). A total of 1 (0.01%), 4 (0.4%), 1 (0.01%) and 7 (0.6%) data points were discarded for WBSF, IMF, cook-loss and pH_u respectively. From this point forward, identified outliers are excluded from calculations and results, including computation of descriptive statistics.

Fluorescence background and multiplicative effects introduced by variations in experimental conditions such as laser intensity fluctuations were removed by means of pre-processing techniques. Several methods were trialled including baseline correction followed by unit vector normalisation (UVN), baseline correction followed by standard normal variate (SNV), Savitzky-Golay (SG) derivation, extended multiplicative scattering correction (EMSC) and EMSC with replicate correction. Baseline correction was performed using the *baseline.modpolyfit* command of the R *baseline* package with a 5th order polynomial. The algorithm is based on the method developed by Lieber & Mahadevan-Jansen which is a modification to least-squares polynomial curve fitting (Lieber & Mahadevan-Jansen, 2003). SG derivation was applied using first and second derivatives. The former with a third-degree polynomial and the latter with a second-degree polynomial. Both SG approaches were applied using 9 smoothing points. EMSC with replicate correction

was trialled to reduce the variation between replicates. Briefly, EMSC with replicate correction generates individual EMSC models for each set of replicates and uses principal component analysis to estimate the variation between replicates of the data set (Afseth & Kohler, 2012; Liland, Kohler, & Afseth, 2016). EMSC techniques were applied using the mean spectrum of the dataset as reference and a six-degree polynomial. After pre-processing, spectral scans/replicates recorded per sample were averaged. For most samples the average was based on 10 scans, yet, for those samples that 1 or 2 replicates (i.e. spectral outliers) had been discarded, the average was based on the remaining 9 or 8 scans.

Partial least squares (PLS) regression was used to correlate the spectral data to the reference values measured for each quality indicator. Cross validation (CV) was carried out using 10 randomly-selected data splits with 20 iterations. Variable importance in projection (VIP) was used to discard spectral bands which were not relevant for the prediction of each quality indicator. VIP was applied with a 0.9 threshold and using an in-house algorithm which iteratively selected the most important Raman bands and fitted new PLS models until reaching a global minimum of root mean square error of cross-validation (RMSECV). A similar algorithm was used in other studies (Bauer et al., 2016; Scheier et al., 2014). Selection of the optimal number of latent variables (LV) was based on the RMSECV since it provides information about the deviation of the model from their reference values (Cama-Moncunill et al., 2017). For that, RMSECV values were displayed as a function of the number of LV used in the models. From the plot (not shown), models with the lowest RMSECV were selected and subsequently inspected for overfitting. If little improvement was found when compared to models with fewer LV, models with fewer LV were selected.

PLS models were first developed using the complete data set and then using train sets comprising 90% of the samples. PLS models were assessed through various figures of merit. In the frame of calibration, models were evaluated through the coefficients of determination of calibration (R^2) and the root mean square error of calibration (RMSEC) computed from the correlation of the spectral data to the variation of meat quality. Models developed with the complete data set were further appraised by the coefficient of determination of cross-validation (R^2cv) and the RMSECV both computed from the cross-validation step with 20 iterations, together with the coefficient of determination (r^2), bias and slope computed from the correlation between predicted and measured values. The loading values provided for these models were used to evaluate the principal bands contributing to the prediction of each quality trait. In order to assess the predictive ability of the approach, data was randomly split into train and test sets 3 times using a sample split of 90/10. Train sets were used to build PLS models and test sets to evaluate the predictive ability of the models. For that, the root mean square error of prediction (RMSEP) was used along with the residual prediction deviation (RPD) and the range error ratios (RER). RPD is defined as the ratio between the standard deviation of the reference values and the RMSEP, while RER as the ratio between the range in the reference values of the validation set and the RMSEP (Williams & Norris, 2001).

3. Results and discussion

3.1. Meat quality data

Descriptive statistics for each beef quality indicator are presented in Table 1. The sample set presented typical pH_u values for beef ranging from 5.34 to 5.8 (Honikel, 2014). WBSF ranged from 22.05 to 71.4 N; thus, encompassing a range including tender, intermediate and tough samples (Shackelford et al., 1991). The sample set also presented a reasonable spread in IMF, ranging from 0.07% to 5.4%, which would be in the typical range of variation for Irish beef (Cafferky et al., 2019). Based on the coefficient of variation (CoV), it was considered that

Table 1

Descriptive statistics computed for each of the beef quality indicators.

	N	Mean	SD	Median	Min	Max	CoV (%)
UpH (pH units)	102	5.53	0.09	5.53	5.34	5.8	1.6
WBSF (N)	109	43.93	10.35	43.48	22.05	71.4	23.6
IMF (%)	89	1.92	1.34	1.56	0.07	5.36	69.8
Drip-loss (%)	81	2.89	1.17	2.86	0.71	5.27	40.5
Cook-loss (%)	109	28.81	3.1	28.63	22.03	35.2	10.8

N: number of beef samples.

SD: standard deviation.

CoV: coefficient of variation.

UpH: ultimate pH.

WBSF: Warner-Bratzler shear force.

IMF: intramuscular fat.

sufficient variability existed within WBSF, IMF, drip-loss and cook-loss data to develop models with the Raman spectral set (Cafferky et al., 2019), but not for ultimate pH.

3.2. PLSR models for predicting objective quality traits

To evaluate the potential of Raman spectroscopy to provide quantitative information on beef quality, PLSR models were developed for each quality indicator using various pre-processing techniques and Raman shift ranges. A summary of the best two models developed for each quality trait is shown in Table 2. The rest of the models are presented in Annexe 1. In general, models exhibited notable model fit (R^2 ranging from approx. 0.48 to 0.91 and low RMSEC) and different levels of accuracy when cross-validated (R^2cv ranging from approx. 0.34 to 0.64). Furthermore, models resulted in increased predictive ability when based on the Raman shift ranges from 1800 to 700 cm^{-1}, rather than 3100–700 cm^{-1}. This effect was attributed to the fact that most relevant Raman scattering responses of meat occur within the range from 1800 to 500 cm^{-1} (Fowler et al., 2014a).

Prior to model building, a preliminary investigation of the spectral data was performed with the aim to determine the most relevant Raman bands for beef as well as identify the variability in the Raman data related to the variation within each meat-quality attribute. Fig. 1 shows the average spectra of the 5 samples with the lowest (in red) and the average spectra of the 5 samples with the highest (in black) values

determined for IMF, WBSF, drip-loss and Cook-loss. To facilitate interpretation, baseline corrected followed by UVN spectra are displayed. All spectra presented the characteristic Raman signal of proteins—broad and dominant bands due to vibrations from multiple peptides and amino acids (Socrates, 2004; Tuma, 2005). Peptide backbone signals are observed at the regions of 1685–1645 cm^{-1} (amide I band), 1340–1225 cm^{-1} (amide III band), together with various bands within the region of 1130–800 cm^{-1} (C–C, C–N and CNC stretching) and at 1450 cm^{-1} (C–H deformations) (Benevides, Overman, & Thomas Jr., 2003; Herrero, 2008; Schmidt et al., 2013; Socrates, 2004). The signal at 935 cm^{-1} (C–C stretching of α-helical structures) along with the amide I band centred at 1655 cm^{-1} and the amide III doublet at 1318 and 1270 cm^{-1} indicated that α-helical structures predominated (Ana M. Herrero, 2008). Aromatic amino-acid responses included signals from: tryptophan (Trp) at 1553, 1341, 880 and 752 cm^{-1} (Bauer et al., 2016; Benevides et al., 2003; Tuma, 2005); phenylalanine (Phe) at 1003 cm^{-1} (Beattie et al., 2004); and tyrosine (Tyr) at 855 and 825 cm^{-1} (Fowler, Schmidt, Van de Ven, et al., 2014). Furthermore, the shoulder band at approx. 1615 cm^{-1} was associated with Phe and Tyr (Benevides et al., 2003); while the peak at 1402 was attributed to C=O stretching of the COO– group in aspartic and glutamic acids (E. Li-Chan, Chalmers, & Griffiths, 2010).

3.2.1. Prediction of WBSF

Comparison between the most tender and toughest beef samples (Fig. 1a) revealed few obvious spectral differences. These differences were observed mainly at the amide I, amide III and 1000–900 cm^{-1} (C–C stretching), where tough samples displayed slightly higher intensity at bands associated with β-sheet (1668 cm^{-1}) and random coil (960 cm^{-1}) conformations (Beattie et al., 2004). Small differences were also observed at 1341 cm^{-1} (Trp) and 825 cm^{-1} (Tyr). The former may indicate changes in the hydrophobicity of the indolyl ring environment; while the latter may indicate changes in the OH hydrogen-bonding state (Benevides et al., 2003). Both therefore, may suggest changes in the tertiary structures of proteins (Ana M. Herrero, 2008).

The best model for WBSF presented modest performances in both calibration (R^2 = 0.48, RMSEC = 7.40 N) and cross-validation (Rcv^2 = 0.36, RMSECV = 8.24 N) (Table 2). The correlation between the cross-validated predictions and the reference values are shown in Fig. 2a. The plot revealed poor fit (r^2 = 0.37) and considerable deviation from the true line (slope = 0.38). Similar results were obtained

Table 2

Summary of the best two PLSR models developed for each beef quality indicator using the complete data set.

Attribute	N	Pre-processing	var	lv	R^2c	RMSEC	R^2cv	RMSECV	RPDcv	RERcv
			Calibration				Cross-Validation			
WBSF	109	EMSC - rep	97	1	0.48	7.40	0.36	8.24	1.3	6.0
		SG1d3p9w	132	2	0.55	6.93	0.34	8.34	1.2	5.9
IMF	89	BSL + UVN	480	4	0.89	0.45	0.64	0.80	1.6	6.6
		BSL + SNV	487	4	0.91	0.40	0.64	0.80	1.6	6.6
Drip-loss	81	SG1d3p9w	224	3	0.88	0.41	0.59	0.74	1.6	6.2
		SG2d2p9w	111	2	0.73	0.60	0.56	0.78	1.5	5.9
Cook-loss	109	SG1d3p9w	427	2	0.67	1.78	0.49	2.21	1.4	6.0
		BSL + UVN	198	3	0.69	1.73	0.47	2.24	1.4	5.9

N: number of beef samples.

var: number of spectral variables retained by VIP.

lv: number of latent variables/PLS factors included in the model.

RPDcv: residual prediction deviation calculated as SD/RMSECV.

RERcv: range error ratio calculated as range/RMSECV.

WBSF: Warner-Bratzler shear force.

IMF: intramuscular fat.

EMSC – rep: extended multiplicative scattering correction with replicate correction.

BSL + SNV: baseline correction followed by standard normal variate.

BSL + UVN: baseline correction followed by unit vector normalisation.

SG1d3p9w: Savitzky-Golay transformation with first derivative, third-degree polynomial and 9 smoothing points.

SG2d2p9w: Savitzky-Golay transformation with second derivative, second-degree polynomial and 9 smoothing points.
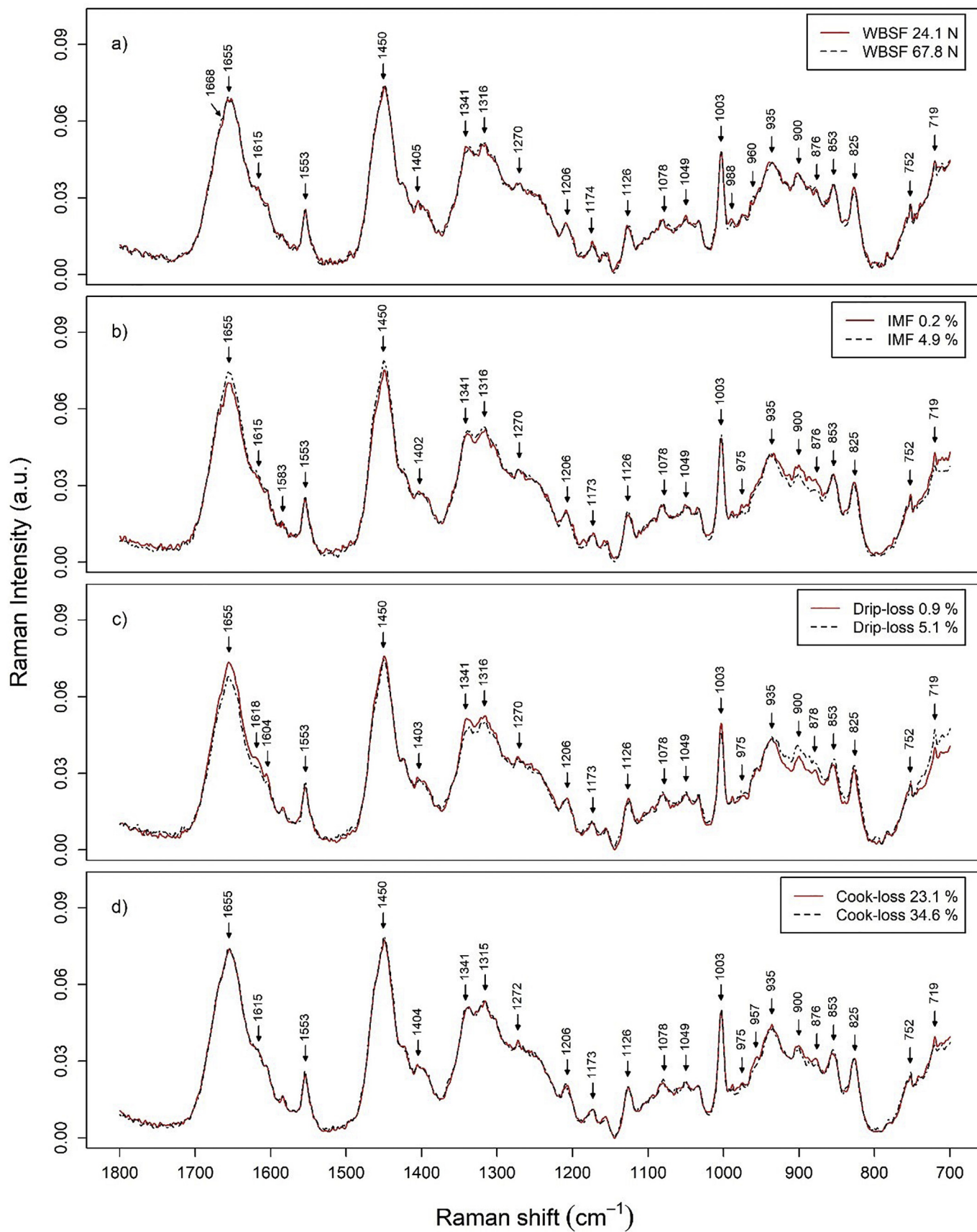
Fig. 1. Baseline corrected and unit vector normalised average spectra of the 5 samples with lowest and highest values of (a) IMF, (b) WBSF, (c) Drip-loss and (d) Cook-loss.
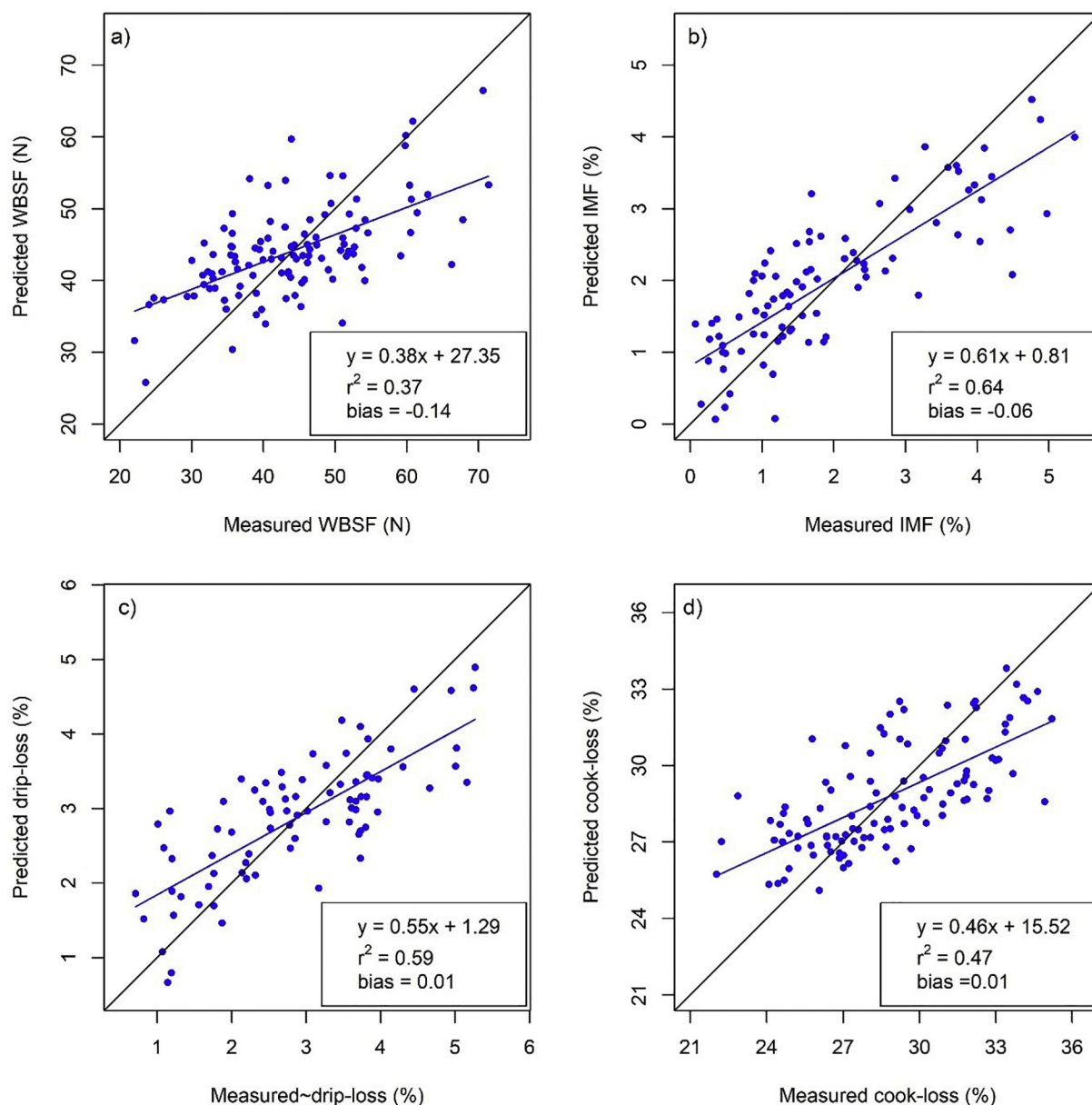
Fig. 2. Measured versus predicted values for (a) WBSF, (b) IMF, (c) drip-loss and (d) cook-loss using the selected models for each quality indicator.

in cross-validation when data was split into train and test sets, with R^2cv ranging from 0.27 to 0.32 and RMSECV from 8,69 to 8,98 N (Table 3). The RMSEP values varied from 4.55 to 9.07 N, indicating an important variability between the results provided by each of the 3 test data sets. Two further figures of merit were used to assess the predictive ability of a models: RPD and RER. As a general rule, RPD and RER values higher than three and twelve, respectively, are considered to be fair and appropriate for screening purposes, while RPD values in the range from 2.4 to 3 and RER values between 7 and 12 are recommended for rough screening purposes (Williams & Norris, 2001). WBSF models presented RDP and RER values ranging from 1.1 to 2.3 and 5.4 to 10.9, respectively. Focussing on the former, an RPD of 1.1 indicates that the RMSECV is nearly as large as the SD of the data set which means that the model has very poor predictive ability (Williams, 2014; Williams & Norris, 2001); while an RPD of 2.3, which is close to the 2.4 threshold, may indicate that the model is appropriate for rough screening purposes. Due to this variability in the results, it is difficult to evaluate the true predictive ability of the approach. These results agreed with previous studies on predicting instrumental tenderness which reported

models for shear force with an R^2 of 0.49 and an R^2cv 0.33 (Bauer et al., 2016); and for WBSF with an R^2 of 0.75 and an RMSECV of 19.8% of the mean (18.8% for our model).

A distinctive aspect of the WBSF model was that only 1 PLS factor was included. This effect was attributed to the pre-processing technique. EMSC with replicate correction reduces the variation between replicates and consequently fewer PLS factors are required to explain the variation within the data set (Afseth & Kohler, 2012). The PLS factor explained 10% of the spectral variance and 48% of the WBSF variance. This indicated that the model accounted for the variation of WBSF, yet the low value of explained spectral variance suggested that most of the spectral variation seen in the data set was not related to the changes in WBSF.

Further model evaluation was conducted through the loading values obtained for the first PLS factor (Fig. 3a) as the plot provides information on the retained Raman bands that contributed to each PLS factor (Cama-Moncunill et al., 2017). The plot disclosed a series of contributing bands which could be attributed to changes in the secondary and tertiary structures of proteins. For example, most bands

Table 3
Summary of the best two PLSR models developed for each beef quality indicator- using train and test sets resulting from a 90/10 data split.

Attribute	Pre-processing	Split	n_c	var	lv	R^2c	RMSEC	R^2cv	RMSECV	n_t	RMSEP	RPD	RER
WBSF	EMSC - rep	1	98	130	1	0.44	7.75	0.30	8.69	11	9.07	1.1	5.4
		2	98	137	1	0.39	8.16	0.27	8.98	11	8.35	1.2	5.9
		3	98	129	1	0.47	7.74	0.32	8.77	11	4.55	2.3	10.9
	SG1d3p9w	1	98	86	2	0.56	6.85	0.37	8.25	11	11.94	0.9	4.1
		2	98	89	2	0.52	7.24	0.35	8.45	11	11.13	0.9	4.4
		3	98	93	2	0.55	7.11	0.35	8.59	11	8.09	1.3	6.1
IMF	BSL + SNV	1	80	380	3	0.83	0.56	0.62	0.86	9	0.88	1.5	6.0
		2	80	395	4	0.89	0.45	0.65	0.81	9	0.94	1.4	5.7
		3	80	378	3	0.82	0.58	0.57	0.87	9	1.14	1.1	4.7
	BSL + UNV	1	80	360	3	0.83	0.57	0.60	0.88	9	0.91	1.4	5.8
		2	80	402	4	0.89	0.46	0.63	0.83	9	0.89	1.5	5.9
		3	80	367	3	0.83	0.55	0.62	0.82	9	1.09	1.2	4.9
Drip-loss	SG1d3p9w	1	72	164	2	0.82	0.50	0.69	0.66	9	1.00	1.2	4.6
		2	72	136	3	0.82	0.48	0.51	0.80	9	1.29	0.9	3.6
		3	72	126	2	0.65	0.67	0.40	0.88	9	1.27	0.9	3.6
	SG2d2p9w	1	72	129	3	0.81	0.53	0.46	0.88	9	0.99	1.2	4.6
		2	72	131	2	0.74	0.58	0.50	0.80	9	1.30	0.9	3.5
		3	72	130	3	0.87	0.42	0.55	0.77	9	1.00	1.2	4.6
Cook-loss	SG1d3p9w	1	98	349	2	0.69	1.66	0.52	2.08	11	2.90	1.1	4.6
		2	98	333	2	0.68	1.77	0.50	2.21	11	1.50	2.1	8.8
		3	98	331	2	0.68	1.78	0.52	2.17	11	2.30	1.4	5.8
	BSL + UVN	1	98	135	2	0.50	2.13	0.36	2.41	11	3.19	1.0	4.1
		2	98	128	3	0.62	1.92	0.40	2.42	11	2.35	1.3	5.6
		3	98	118	3	0.60	1.98	0.43	2.38	11	2.04	1.5	6.5

Split: each of the 3 random splits generated.
nc: number of beef samples in train data set.
nt: number of beef samples in test data set.
var: number of spectral variables retained by VIP.
lv: number of latent variables/PLS factors included in the model.
RPD: residual prediction deviation calculated as SD/RMSEP.
RER: range error ratio calculated as range/RMSEP.
WBSF: Warner-Bratzler shear force.
IMF: intramuscular fat.
EMSC – rep: extended multiplicative scattering correction with replicate correction.
BSL + SNV: baseline correction followed by standard normal variate.
BSL + UVN: baseline correction followed by unit vector normalisation.
SG1d3p9w: Savitzky-Golay transformation with first derivative, third-degree polynomial and 9 smoothing points.
SG2d2p9w: Savitzky-Golay transformation with second derivative, second-degree polynomial and 9 smoothing points.

from 1680 to 1665 cm^{-1} (β-sheet) were positively correlated to WBSF which agreed with Beattie et al. (2004) who suggested that tough meat presents a larger amount of β-sheet structures compared to tender meat. Furthermore, the band at 960 cm^{-1} (C–C stretching vibrations of random coil structures) also presented a positive correlation to WBSF (Beattie et al., 2004; Ana M. Herrero, 2008). Yet, the contribution of α-helical structures—typically assigned at approx. 1655, 1320–1305, 1273 and 935 cm^{-1}—was unclear as a mixture of bands with positive and negative relationships were observed. This effect could be due to changes in the signals of α-helical structures as its response dependents on sample orientation (Pézolet, Pigeon, Ménard, & Caillé, 1988). The region at 800–900 cm^{-1}, which is associated with the symmetrical CNC stretching vibration of proteins (Socrates, 2004), was also positively correlated to WBSF. Interestingly, other studies related the signal at 855 cm^{-1} to connective tissue (Bauer et al., 2016). However, this association could not be confirmed due to unclear contribution from other connective tissue bands such as 1270 and 1248 cm^{-1} (Bauer et al., 2016).

Regarding changes in the tertiary structure of proteins, the bands at 1552 and 1339 cm^{-1} could arise from tryptophan signals (Schmidt et al., 2013). Particularly, the band at 1339 cm^{-1} is sensitive to the hydrophobicity of the local environment and can be used to provide information on how buried the tryptophan residue is within the protein network (Benevides et al., 2003; Ana M. Herrero, 2008; Xu, Han, Fei, & Zhou, 2011). However, other tryptophan signals (e.g. 880 and 760 cm^{-1}) had no contribution to the loading values. Therefore, the

relationship between WBSF and tryptophan residues/hydrophobic characteristics could not be confirmed. In addition, the band at 1405 cm^{-1}, negatively correlated to WBSF, could be due to the C=O stretching of aspartic and glutamic acids.

Overall, the loading plot displayed a series of contributing bands which are likely to arise from changes in WBSF. However, the plot also illustrated the contribution from bands not readily interpreted. This result together with the small differences observed between the spectra of tough and tender meat (Fig. 1a) suggested that signals not related to physico-chemical changes were included in the model, which in fact could explain the relatively low values of R^2 and R^2cv of the model.

3.2.2. Prediction of IMF

Several spectral differences were observed between samples with the lowest and highest levels of IMF (Fig. 1b). Samples with higher IMF content presented greater intensity values at 1655, 1450, 1316 and 1126 cm^{-1}. Higher intensity at the amide I band (1685–1645 cm^{-1}) may be due to contribution from lipids such as the C=C stretching mode occurring around 1680–1640 cm^{-1} (Herrero, 2008; Li-Chan et al., 2010); while the increase at 1450 cm^{-1} may be due to CH_3, CH_2 and CH bending modes of lipids (Berhe et al., 2014; Herrero, 2008; Tuma, 2005). Similarly, the intensity increase at 1316 cm^{-1} could be related to CH_2 twisting modes of lipids (Fowler et al., 2018; Nian et al., 2017; Zhao et al., 2018); while the increase at 1126 cm^{-1} could be associated to C–C stretching modes (Fowler, Ponnampalam, Schmidt, Wynn, & Hopkins, 2015). Contrarily, the spectrum for the lowest IMF
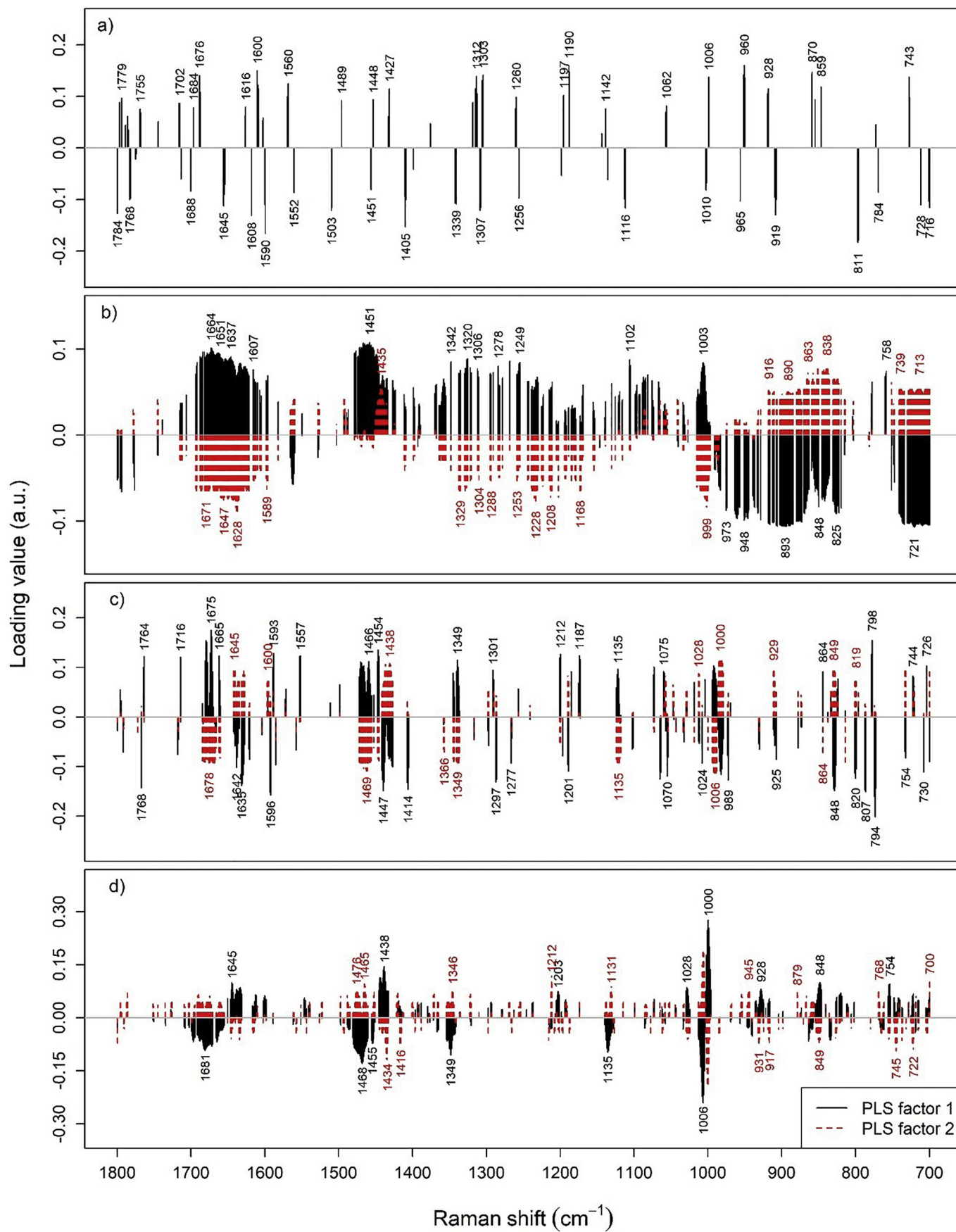
Fig. 3. Loading values of first/first two PLS factors employed by the selected models for: (a) WBSF, (b) IMF, (c) drip-loss and (d) cook-loss.

samples presented greater intensity at 975, 900 and 876 cm^{-1}. These bands were tentatively assigned to protein signals arising from C–C and CNC stretching modes (Beattie et al., 2004; Socrates, 2004).

The best PLSR model developed for IMF presented excellent model fit (R^2 = 0.89, RMSEC = 0.45%) and notable predictive ability (R^{2}cv = 0.64, RMSECV = 0.8%) (Table 2). The correlation between the cross-validated predictions and the references values (Fig. 2b) revealed considerable fit (r^2 = 0.64) and modest deviation from the true line (slope = 0.6). PLS models developed using train sets (Table 3) also exhibited notable performances in calibration (R^2 range = 0.71–0.82, RMSEC range = 0.62–0.77%) and in cross-validation (R^{2}cv range = 0.46–0.52, RMSECV range = 0.97–1.05%). RMSEP values presented notable variability (0.89–1.35%), giving rise to RPD values between 1.1 and 1.5 and RER between 4.7 and 6 (Table 3). While still regarded as poor predictive ability according to the general classification of RPD by Williams and Norris (2001), other authors—including Williams—indicated that for models of complex samples an RPD > 2 (Williams, 2014) and even > 1.5 (D'Acqui, Pucci, & Janik, 2010; Kyprianidis & Skvaril, 2017) may still be usefull for preliminary applications. However, the variability observed in RMSEP, RPD and RER between the 3 different splits makes it difficult to accurately evaluate the predictive ability of the approach. In general, results are in agreement with a previous study on porcine meat which reported a R^{2}cv of 0.73 and RPDcv—computed using RMSECV rather than RMSEP—of 1.9 (Andersen et al., 2018).

The IMF model was based on 4 PLS factors which combined explained 57% of the spectral variance and 91% of the IMF variance indicating that the model accounted for most of the IMF variation within the data set. Further model evaluation was conducted through the loading values obtained for the first two PLS factors (Fig. 3b). The loading values of the first factor exhibited similar features to those observed in the spectral plot comparing the samples with highest and lowest IMF levels (Fig. 1b). This included contribution from the amide I (1685–1645 cm^{-1}) and III (1320–1225 cm^{-1}) bands, various C–H vibration modes (1450 cm^{-1}) and C–C stretching modes (1126–1030 cm^{-1}). As indicated in Fig. 1b, the involvement of the amide I and III regions may be due contribution from lipids such as C=C stretching (1660–1640 cm^{-1}), CH$_2$ twisting (1300 cm^{-1}) and C–H deformations (1270 cm^{-1}) (Fowler, Schmidt, et al., 2015; Nian et al., 2017; Socrates, 2004).

As for the loading values of the second factor, the plot indicated that a great part of the Raman bands contributing to the first factor also contributed to the second factor with inverse relationship. However, the second factor also revealed a positive correlation with a series of bands such as at 1435, 1080 and 1061 cm^{-1} which could be related to vibration modes of lipids. For instance, the region around 1438 cm^{-1} has been associated with CH$_2$ scissoring modes and the bands at 1080 and 1068 cm^{-1} with C–C stretching modes, both of the aliphatic chains of lipids (Chen et al., 2018; Fowler, Ponnampalam, et al., 2015; Zhao et al., 2018). Overall, the plot indicated that most of the lipid-related bands (e.g. 1435 and 1126–1030 cm-1) contribute to the IMF model with a positive correlation. However, the plot also indicated contribution from non-readily identified bands which may not be related to the variation of IMF. This effect may explain the modest spectral variance explained (57%) by the model.

3.2.3. Prediction of drip-loss and cook-loss

Comparison among samples with the lowest and highest drip-loss (Fig. 1c) disclosed several spectral differences. Samples with the lowest drip-loss presented greater intensity values at the amide I and amide III bands as well as at various bands assigned to tyrosine and phenylalanine such as 1618, 1605 and 1003 cm^{-1} (Benevides et al., 2003; Li-Chan, Chalmers, & Griffiths, 2010). Samples with the highest drip-loss exhibited greater intensity at 1553 and 876 cm^{-1} which could be assigned to tryptophan (Bauer et al., 2016; Schmidt et al., 2013); yet, the band at 876 cm^{-1} together with the band at 900 cm^{-1} could be

attributed to C–C and CNC stretching modes of proteins (Socrates, 2004). Comparison between the spectra recorded for samples with the lowest and highest cook-loss (Fig. 1d) displayed little differences, which for the most part were observed at the region between 1000 and 870 cm^{-1} where samples with lowest cook-loss presented slightly higher intensity values.

Drip-loss and cook-loss models presented notable fit with R^2 values of 0.88 and 0.67, and RMSEC values of 0.41% and 1.78%, respectively (Table 2). The R^{2}cv and RMSECV obtained for the drip-loss model were 0.59 and 0.74%, while for the cook-loss models the R^{2}cv was 0.49 and the RMSECV was 2.21%. The correlations between cross-validated predictions and references values for drip-loss and cook-loss are displayed in Fig. 2.c and d, respectively. Both correlation plots revealed considerable fit (r^2 = 0.59 for drip-loss, r^2 = 0.47 for cook-loss) and deviation from the true line (slope = 0.55 for drip-loss, slope = 0.46 for cook-loss). For drip-loss, the test with independent samples (Table 3) provided similar and promising results in cross-validation (R^{2}cv = 0.40–0.69, RMSECV = 0.66–0.88%); however, it also indicated limited predictive ability with RMSEP values ranging from 0.99 to 1.30%, RPD from 0.9 to 1.2 and RER from 3.5 to 4.6. Similarly, cook-loss models exhibited notable performances in cross-validation (R^{2}cv = 0.50–0.52, RMSECV = 2.08–2.21%), yet, more variability was observed in validation: RMSEP ranging from 1.50–2.90%, RPD from 1.1 to 2.1 and RER from 4.6 to 8.8. Compared to a previous study on porcine meat (Scheier et al., 2014), the drip-loss model exhibited less predictive ability (R^{2}cv pork = 0.73). This difference, however, was associated to a greater drip-loss variation across the sample set. The study by Scheier et al. (2014) evaluated a sample set ranging from 0.7 to 9.2% of drip-loss, while in this study the range was 0.7–5.3%. As for the cook-loss model, results indicated better performances than those reported in previous studies such as the work by Fowler, Schmidt, et al. (2015) and Schmidt et al. (2013). Nevertheless, their work was performed in situ using a portable Raman system.

The drip-loss model was built using 3 PLS factors, which combined explained 88% of the variation in drip-loss and 40% of the spectral variance; while the cook-loss model utilized 2 PLS factors explaining 64% of the variation in cook-loss and 39% of the spectral variance. The loading values for the first two PLS factors of the drip-loss model are displayed in Fig. 3c. In general, the loading values for the first factor agreed with the spectral differences observed in Fig. 1c. The first factor indicated that β-sheet and random coil structures in the amide I region had a positive correlation to drip-loss; while the α-helix region exhibited a negative correlation. Raman scattering due to vibrations of other molecular species may occur near the α-helix bands of the amide I region. For example, O–H bending from water molecules occurs at 1640 cm^{-1} (Socrates, 2004). Although water has a relatively weak Raman response, contribution from water around 1640 cm^{-1} could be considered as the loading plot displayed a clear inverse relationship between drip-loss and the bands near 1642 cm^{-1}. In addition, signals of tyrosine and phenylalanine are assigned near the α-helix region. Focusing on the former, the tyrosine doublet (848 and 820 cm^{-1}) also presented a negative correlation to drip-loss.

Loading values of the cook-loss model (Fig. 3d) exhibited a similar profile of contributing bands to those observed for the drip-loss model with some variations. One of the main differences was observed on the contribution of some Raman bands related to secondary structures. For example, the β-sheet band at 1680 cm^{-1} appeared to be negatively correlated with cook-loss, however positively correlated with drip-loss. Similarly, α-helical bands such as 1645 and 928 cm^{-1} were positively correlated with cook-loss; while the bands were negatively correlated with drip-loss. As for drip-loss, bands near 1640 cm^{-1} in which water may have had involvement, had contribution to the loading values, yet with a positive correlation to cook-loss. On the contrary, the tyrosine doublet was not as relevant as it was for the drip-loss model; whilst phenylalanine bands, especially the signal at 1003 appeared to relatively contribute to both factors. Nevertheless, both drip-loss and cook-

loss loading values displayed that the band at 1414 cm^{-1} had contribution. This band could arise from CO_2^- stretching modes of aspartic and glutamic and acids, which play an important role in binding water (Li-Chan, Griffiths, & Chalmers, 2010; Warner, 2017; Xu et al., 2011). Finally, Scheier et al. (2014), who used a portable Raman system to predict drip-loss of pork measured between 60 and 120 min *post-mortem*, thus during *pre-rigor mortis*, found that components involved on the energy metabolism of muscles (e.g. lactate, glycogen, adenosine diphosphate (ADP), adenine and creatine) had contribution to their drip-loss model. However, overall these components had little contribution to the drip-loss models probably because Raman measurements were performed on beef aged for 2 days, at the end of *rigor mortis*. After *rigor mortis*, these components are metabolized to inosine monophosphate (IMP) (Honikel, 2014b). Thus, the bands at 1553 and 720 cm^{-1} could be related to signals of IMP (Scheier et al., 2014).

Overall, the loading plot demonstrated that both models were based on changes in the secondary and tertiary structures of proteins. It also suggested that the contribution of these bands may be slightly different for predicting drip-loss or cook-loss. However, these differences may arise from the experimental design as drip-loss was measured on fresh muscle, while Raman acquisition and cook-loss were performed on thawed muscle. Furthermore, drip-loss and Raman spectra were measured on steaks aged for 2 days; while cook-loss were measured on steaks aged for 14 days. As observed for WBSF and IMF, the loading values for drip-loss and cook-loss indicated that Raman bands not readily identified had contribution to the model. Thus, models may be influenced by bands that may not be related to the physico-chemical variation of the samples, affecting the accuracy of the predictions.

In all, promising prediction models were developed for WBSF, IMF, drip-loss and cook-loss. However, validation with independent sample sets revealed noticeable variability in the results making it difficult to assess the true predictive ability of the models. This variability could be caused by the limited sample size, thereby making results highly dependent on the train-test split. For this reason, future studies should allow for a larger independent test data set to accurately assess the predictive ability of the calibration models.

4. Conclusion

Raman spectroscopy followed by chemometrics constitutes a promising methodology for fast assessment of objective beef quality traits. Notable spectral quality was obtained between the Raman shift range from 1800 to 700 cm^{-1}, which covers the main spectral features related to changes in meat quality indicators such as WBSF, IMF, drip-loss and cook-loss. Overall, PLS models exhibited notable performances in calibration, especially for IMF, drip-loss and cook-loss, and despite the limited sample size, models showed reasonable predictive ability. Furthermore, evaluation of the loading values demonstrated that models were considerably based on the variation of meat quality. Tentative interpretation of the loading plots suggested that changes in IMF would be associated with Raman signals arising from C–C and C=C stretching, CH$_2$ twisting and various vibrations modes of CH; while changes in Warner-Bratzler shear force, drip-loss and cook-loss would be related to changes in the secondary protein structures (α-helix, β-sheet and random coils), hydrophobicity of the myofibrillar environment (tryptophan signals), hydrogen-bonding state (tyrosine doublet) and signals from aspartic and glutamic acids. The loading plots also disclosed that Raman bands a priori not related to the variation of meat quality had contribution to the predictive models. This effect together with overall results denoted that further improvement is required in order to enhance the accuracy of the method.

Nonetheless, promising calibration models were developed and hence further development of the technique is encouraged, especially since Raman spectroscopy is rapid, non-invasive and offers the possibility to use probes and portable systems, making the technology suitable for in situ measurements of beef eating quality at early stages post-mortem. In addition, Raman spectroscopy provides information on an individual basis (e.g. each measured steak). This aspect not only is relevant to meat processors, who could use the information for quality control and hence guarantee consistent quality and consumer satisfaction; but also to consumers as this information could be included in the product label providing information about its expected eating quality. Furthermore, this information has potential to be used in breeding programmes for the improvement of beef eating quality.

Declaration of Competing Interest

The authors declare they have no competing interests.

Appendix A. Supplementary data

Supplementary data to this article can be found online at https://doi.org/10.1016/j.meatsci.2020.108157.

References

Afseth, N. K., & Kohler, A. (2012). Extended multiplicative signal correction in vibrational spectroscopy, a tutorial. *Chemometrics and Intelligent Laboratory Systems, 117*, 92–99. https://doi.org/10.1016/j.chemolab.2012.03.004.

American Meat Science Association (AMSA) (2015). *Research guidelines for cookery, sensory evaluation, and instrumental tenderness measurements of meat* (2nd ed.). Champaign, Illinois: American Meat Science Association Educational Foundation.

Andersen, P. V., Wold, J. P., Gjerlaug-Enger, E., & Veiseth-Kent, E. (2018). Predicting post-mortem meat quality in porcine longissimus lumborum using Raman, near infrared and fluorescence spectroscopy. *Meat Science, 145*, 94–100. https://doi.org/10.1016/j.meatsci.2018.06.016.

AOAC International (1995). In P. Cunniff (Ed.). *Official methods of analysis of AOAC International*(16th ed.). Arlington, VA: AOAC International.

Barbera, S. (2019). WHCtrend, an up-to-date method to measure water holding capacity in meat. *Meat Science, 152*, 134–140. https://doi.org/10.1016/j.meatsci.2019.02.022.

Bauer, A., Scheier, R., Eberle, T., & Schmidt, H. (2016). Assessment of tenderness of aged bovine gluteus medius muscles using Raman spectroscopy. *Meat Science, 115*, 27–33. https://doi.org/10.1016/j.meatsci.2015.12.020.

Beattie, R. J., Bell, S. J., Farmer, L. J., Moss, B. W., & Patterson, D. (2004). Preliminary investigation of the application of Raman spectroscopy to the prediction of the sensory quality of beef silverside. *Meat Science, 66*(4), 903–913. https://doi.org/10.1016/j.meatsci.2003.08.012.

Benevides, J. M., Overman, S. A., & Thomas, G. J., Jr. (2003). Raman spectroscopy of proteins. *Current Protocols in Protein Science, 33*(1), 17.8.1–17.8.35. https://doi.org/10.1002/0471140864.ps1708s33.

Berhe, D. T., Engelsen, S. B., Hviid, M. S., & Lametsch, R. (2014). Raman spectroscopic study of effect of the cooking temperature and time on meat proteins. *Food Research International, 66*, 123–131. https://doi.org/10.1016/j.foodres.2014.09.010.

Cafferky, J., Hamill, M. R., Allen, P., O'Doherty, V. J., Cromie, A., & Sweeney, T. (2019). Effect of breed and gender on meat quality of *M. longissimus* thoracis et lumborum muscle from crossbred beef bulls and steers. *Foods.* https://doi.org/10.3390/foods8050173.

Cafferky, J., Sweeney, T., Allen, P., Sahar, A., Downey, G., Cromie, A., & Hamill, R. M. (2019). Investigating the use of visible and near infrared spectroscopy to predict sensory and texture attributes of beef *M. longissimus* thoracis et lumborum. *Meat Science,* 107915. https://doi.org/10.1016/j.meatsci.2019.107915.

Cama-Moncunill, R., Casado-Gavalda, M. P., Cama-Moncunill, X., Markiewicz-Keszycka, M., Dixit, Y., Cullen, P. J., & Sullivan, C. (2017). Quantification of trace metals in infant formula premixes using laser-induced breakdown spectroscopy. *Spectrochimica Acta - Part B Atomic Spectroscopy, 135*, 6–14. https://doi.org/10.1016/j.sab.2017.06.014.

Cecchinato, A., De Marchi, M., Penasa, M., Albera, A., & Bittante, G. (2011). Near-infrared reflectance spectroscopy predictions as indicator traits in breeding programs for enhanced beef quality1. *Journal of Animal Science, 89*(9), 2687–2695. https://doi.org/10.2527/jas.2010-3740.

Chen, Q., Xie, Y., Xi, J., Guo, Y., Qian, H., Cheng, Y., ... Yao, W. (2018). Characterization of lipid oxidation process of beef during repeated freeze-thaw by electron spin resonance technology and Raman spectroscopy. *Food Chemistry, 243*, 58–64. https://doi.org/10.1016/j.foodchem.2017.09.115.

Corbin, C. H., O'Quinn, T. G., Garmyn, A. J., Legako, J. F., Hunt, M. R., Dinh, T. T. N., ... Miller, M. F. (2015). Sensory evaluation of tender beef strip loin steaks of varying

marbling levels and quality treatments. *Meat Science, 100*, 24–31. https://doi.org/10.1016/j.meatsci.2014.09.009.

Core Team, R. (2018). *R: A language and environment for statistical computing.* Vienna, Austria: R Foundation for Statistical Computing. http://www.R-project.org/.

D'Acqui, L. P., Pucci, A., & Janik, L. J. (2010). Soil properties prediction of western Mediterranean islands with similar climatic environments by means of mid-infrared diffuse reflectance spectroscopy. *European Journal of Soil Science, 61*(6), 865–876. https://doi.org/10.1111/j.1365-2389.2010.01301.x.

Di Luca, A., Mullen, A. M., Elia, G., Davey, G., & Hamill, R. M. (2011). Centrifugal drip is an accessible source for protein indicators of pork ageing and water-holding capacity. *Meat Science, 88*(2), 261–270. https://doi.org/10.1016/j.meatsci.2010.12.033.

Fowler, S. M., Ponnampalam, E. N., Schmidt, H., Wynn, P., & Hopkins, D. L. (2015). Prediction of intramuscular fat content and major fatty acid groups of lamb *M. longissimus lumborum* using Raman spectroscopy. *Meat Science, 110*, 70–75. https://doi.org/10.1016/j.meatsci.2015.06.016.

Fowler, S. M., Schmidt, H., van de Ven, R., & Hopkins, D. L. (2018). Preliminary investigation of the use of Raman spectroscopy to predict meat and eating quality traits of beef loins. *Meat Science, 138*(August 2017), 53–58. https://doi.org/10.1016/j.meatsci.2018.01.002.

Fowler, S. M., Schmidt, H., van de Ven, R., Wynn, P., & Hopkins, D. L. (2014a). Raman spectroscopy compared against traditional predictors of shear force in lamb *M. longissimus lumborum*. *Meat Science, 98*(4), 652–656. https://doi.org/10.1016/j.meatsci.2014.06.042.

Fowler, S. M., Schmidt, H., Van de Ven, R., Wynn, P., & Hopkins, D. L. (2014b). Predicting tenderness of fresh ovine semimembranosus using Raman spectroscopy. *Meat Science, 97*(4), 597–601. https://doi.org/10.1016/j.meatsci.2014.02.018.

Fowler, S. M., Schmidt, H., van de Ven, R., Wynn, P., & Hopkins, D. L. (2015). Predicting meat quality traits of ovine m. semimembranosus, both fresh and following freezing and thawing, using a hand held Raman spectroscopic device. *Meat Science, 108*, 138–144. https://doi.org/10.1016/j.meatsci.2015.06.010.

Gagaoua, M., Picard, B., Soulat, J., & Monteils, V. (2018). Clustering of sensory eating qualities of beef: Consistencies and differences within carcass, muscle, animal characteristics and rearing factors. *Livestock Science, 214*, 245–258. https://doi.org/10.1016/j.livsci.2018.06.011.

Gremlich, H. U., & Yan, B. (2000). *Infrared and Raman spectroscopy of biological materials.* Taylor & Francis.

de Groot, P. J., Postma, G. J., Melssen, W. J., Buydens, L. M. C., Deckert, V., & Zenobi, R. (2001). Application of principal component analysis to detect outliers and spectral deviations in near-field surface-enhanced Raman spectra. *Analytica Chimica Acta, 446*(1), 71–83. https://doi.org/10.1016/S0003-2670(01)01267-3.

Herrero, A. M. (2008). Raman spectroscopy a promising technique for quality assessment of meat and fish: A review. *Food Chemistry, 107*(4), 1642–1651. https://doi.org/10.1016/j.foodchem.2007.10.014.

Hocquette, J.-F., Van Wezemael, L., Chriki, S., Legrand, I., Verbeke, W., Farmer, L., ... Pethick, D. W. (2014). Modelling of beef sensory quality for a better prediction of palatability. *Meat Science, 97*(3), 316–322. https://doi.org/10.1016/j.meatsci.2013.07.031.

Honikel, K. O. (2014a). Chemical and physical characteristics of meat|pH measurement. In C. Devine, & M. Dikeman (Eds.). *Encyclopedia of meat sciences* (pp. 262–266). (2nd ed.). Oxford: Academic Press.

Honikel, K. O. (2014b). Conversion of muscle to meat|glycolysis. In C. Devine, & M. Dikeman (Eds.). *Encyclopedia of meat sciences* (pp. 353–357). (2nd ed.). Oxford: Academic Press.

Honikel, K. O., & Hamm, R. (1994). Measurement of water-holding capacity and juiciness. In A. M. Pearson, & T. R. Dutson (Eds.). *Quality attributes and their measurement in meat, poultry and fish products* (pp. 125–161). London: Blackie Academic.

Kyprianidis, K., & Skvaril, J. (2017). *Developments in near-infrared spectroscopy.* (IntechOpen).

Li-Chan, E., Chalmers, J. M., & Griffiths, P. R. (2010). *Applications of vibrational spectroscopy in food science.* Wiley.

Li-Chan, E. C. Y., Griffiths, P. R., & Chalmers, J. M. (2010). *Applications of vibrational spectroscopy in food science: Volume I: Instrumentation and fundamental applications.* Chichester: John Wiley & Sons.

Lieber, C. A., & Mahadevan-Jansen, A. (2003). Automated method for subtraction of fluorescence from biological Raman spectra. *Applied Spectroscopy, 57*(11), 1363–1367. https://doi.org/10.1366/000370203322554518.

Liland, K. H., Kohler, A., & Afseth, N. K. (2016). Model-based pre-processing in Raman spectroscopy of biological samples. *Journal of Raman Spectroscopy, 47*(6), 643–650. https://doi.org/10.1002/jrs.4886.

McCarthy, S. N., Henchion, M., White, A., Brandon, K., & Allen, P. (2017). Evaluation of

beef eating quality by Irish consumers. *Meat Science, 132*, 118–124. https://doi.org/10.1016/j.meatsci.2017.05.005.

Modzelewska-Kapituła, M., Kwiatkowska, A., Jankowska, B., & Dąbrowska, E. (2015). Water holding capacity and collagen profile of bovine m. infraspinatus during postmortem ageing. *Meat Science, 100*, 209–216. https://doi.org/10.1016/j.meatsci.2014.10.023.

Nache, M., Hinrichs, J., Scheier, R., Schmidt, H., & Hitzmann, B. (2016). Prediction of the pH as indicator of porcine meat quality using Raman spectroscopy and metaheuristics. *Chemometrics and Intelligent Laboratory Systems, 154*, 45–51. https://doi.org/10.1016/j.chemolab.2016.03.011.

Nian, Y., Zhao, M., O'Donnell, C. P., Downey, G., Kerry, J. P., & Allen, P. (2017). Assessment of physico-chemical traits related to eating quality of young dairy bull beef at different ageing times using Raman spectroscopy and chemometrics. *Food Research International, 99*(June), 778–789. https://doi.org/10.1016/j.foodres.2017.06.056.

Pézolet, M., Pigeon, M., Ménard, D., & Caillé, J. P. (1988). Raman spectroscopy of cytoplasmic muscle fiber proteins. Orientational order. *Biophysical Journal, 53*(3), 319–325. https://doi.org/10.1016/S0006-3495(88)83109-6.

Reardon, W., Mullen, A. M., Sweeney, T., & Hamill, R. M. (2010). Association of polymorphisms in candidate genes with colour, water-holding capacity, and composition traits in bovine *M. longissimus* and M. semimembranosus. *Meat Science, 86*(2), 270–275. https://doi.org/10.1016/j.meatsci.2010.04.013.

Ryabchykov, O., Bocklitz, T., Ramoji, A., Neugebauer, U., Foerster, M., Kroegel, C., ... Popp, J. (2016). Automatization of spike correction in Raman spectra of biological samples. *Chemometrics and Intelligent Laboratory Systems, 155*, 1–6. https://doi.org/10.1016/j.chemolab.2016.03.024.

Scheier, R., Bauer, A., & Schmidt, H. (2014). Early Postmortem prediction of meat quality traits of porcine semimembranosus muscles using a portable Raman system. *Food and Bioprocess Technology, 7*(9), 2732–2741. https://doi.org/10.1007/s11947-013-1240-3.

Schmidt, H., Scheier, R., & Hopkins, D. L. (2013). Preliminary investigation on the relationship of Raman spectra of sheep meat with shear force and cooking loss. *Meat Science, 93*(1), 138–143. https://doi.org/10.1016/j.meatsci.2012.08.019.

Shackelford, S. D., Koohmaraire, M., Whipple, G., Wheeler, T. L., Miller, M. F., Crouse, J. D., & Reagan, J. O. (1991). Predictors of beef tenderness: Development and verification. *Journal of Food Science, 56*(5), 1130–1135. https://doi.org/10.1111/j.1365-2621.1991.tb04718.x.

Socrates, G. (2004). In G. Socrates (Ed.). *Infrared and Raman characteristic group frequencies : tables and charts*(3rd ed.). Chichester: John Wiley & Sons, Ltd.

Troy, D. J., & Kerry, J. P. (2010). Consumer perception and the role of science in the meat industry. *Meat Science, 86*(1), 214–226. https://doi.org/10.1016/j.meatsci.2010.05.009.

Tuma, R. (2005). Raman spectroscopy of proteins: From peptides to large assemblies. *Journal of Raman Spectroscopy, 36*(4), 307–319. https://doi.org/10.1002/jrs.1323.

Vankeirsbilck, T., Vercauteren, A., Baeyens, W., Van der Weken, G., Verpoort, F., Vergote, G., & Remon, J. P. (2002). Applications of Raman spectroscopy in pharmaceutical analysis. *TrAC - Trends in Analytical Chemistry, 21*(12), 869–877. https://doi.org/10.1016/S0165-9936(02)01208-6.

Warner, R. D. (2017). Chapter 14 - the eating quality of meat—IV water-holding capacity and juiciness. In F. B. T.-L. M. S. (Eighth E. Toldrá´ (Ed.) (Ed.). *Woodhead Publishing Series in Food Science, Technology and Nutrition. Lawrie's Meat Science* (pp. 419–459). Woodhead Publishing. https://doi.org/10.1016/B978-0-08-100694-8.00014-5.

Webb, E. C., & O'Neill, H. A. (2008). The animal fat paradox and meat quality. *Meat Science, 80*(1), 28–36. https://doi.org/10.1016/j.meatsci.2008.05.029.

Wilcox, R. R. (2010). In R. R. Wilcox (Ed.) (Ed.). *The Normal curve and outlier detection BT - fundamentals of modern statistical methods: Substantially improving power and accuracy* (pp. 29–45). New York, NY, NY: Springer New York. https://doi.org/10.1007/978-1-4419-5525-8_3.

Williams, P. (2014). The RPD statistic: A tutorial note. *NIR News, 25*, 22–26.

Williams, P., & Norris, K. H. (2001). *Near-infrared technology: In the agricultural and food industries.* (American Association of Cereal Chemists).

Xu, X. L., Han, M. Y., Fei, Y., & Zhou, G. H. (2011). Raman spectroscopic study of heat-induced gelation of pork myofibrillar proteins and its relationship with textural characteristic. *Meat Science, 87*(3), 159–164. https://doi.org/10.1016/j.meatsci.2010.10.001.

Zhao, M., Nian, Y., Allen, P., Downey, G., Kerry, J. P., & O'Donnell, C. P. (2018). Application of Raman spectroscopy and chemometric techniques to assess sensory characteristics of young dairy bull beef. *Food Research International, 107*(February), 27–40. https://doi.org/10.1016/j.foodres.2018.02.007.